19th Australasian Fluid Mechanics Conference
Melbourne, Australia
8-11 December 2014

PIV of a Precessing Cylinder Flow

T. Albrecht[1], P. Meunier[2], R. Manasseh[3], J. M. Lopez[4] and H. M. Blackburn[1]

[1]Department of Mechanical and Aerospace Engineering
Monash University, Victoria 3800, Australia

[2]IRPHE, CNRS, and Aix-Marseille Université, 13013 Marseille, France

[3]Department of Mechanical and Product Design Engineering
Swinburne University of Technology, Victoria 3122, Australia

[4]School of Mathematical & Statistical Sciences
Arizona State University, Tempe, AZ 85287, USA

Abstract

We report new results of PIV measurements of the flow in a precessing cylinder at aspect ratios between 0.457 and 2.615, tilt angles up to 5° and Reynolds numbers ranging from 500 to 46 000. The first Kelvin mode is forced at its first resonance; its shape and saturation amplitude is extracted and found to agree well with theory. Geostrophic motion is observed and quantified.

Introduction

Precession—simultaneous rotation around two axes as sketched in figure 1—is a way to excite inertial waves in rotating flows. It has geophysical relevance, being considered one possible driver for the geo-dynamo, i.e., the creation of Earth's magnetic field. Also, liquid fuel in spin-stabilized spacecraft may be subject to precessional forcing, destabilising the whole spacecraft.

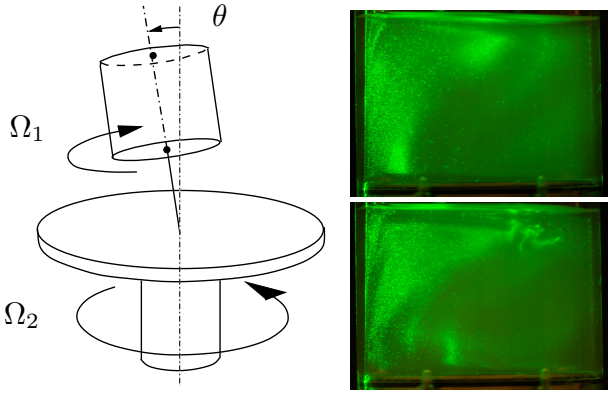

Figure 1. (Left) A cylinder rotates at Ω_1 around its aies, which is tilted by an angle θ with respect to the platform's axis. The platform rotates at Ω_2. (Right) Flow visualizations of the initial, forced mode, and the onset of instability.

Linear, inviscid theory [4] suggests that precessing flow may be decomposed into a sum of Kelvin modes [8]. A Kelvin mode is resonant (i.e. grows to a large amplitude) if its axial wavelength matches the container height. At large enough Reynolds numbers, it may also become unstable. Johnson [3], Malkus [6] and Manasseh [7] observed a rapid transition from laminar to turbulent flow. This so-called catastrophic collapse may be explained by several competing theories: triadic resonance, instability of a Kelvin mode, boundary layer instability, or modification of the base flow by geostrophic motion eventually leading to centrifugal instability. Figure 1 shows typical flow visualizations of the initial mode shape and the onset of instability.

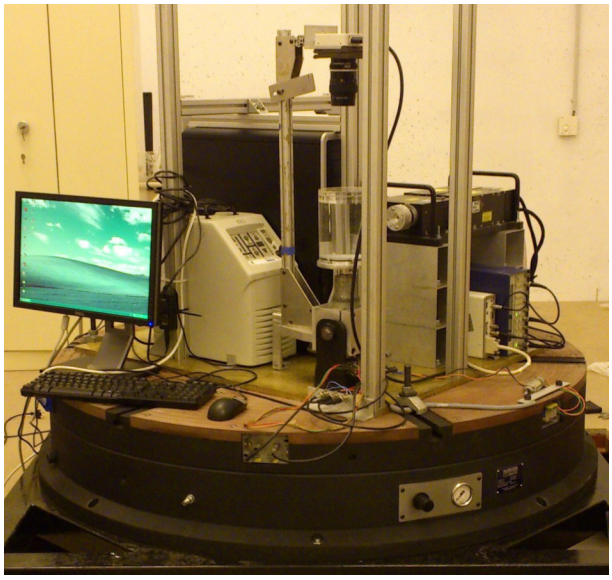

Figure 2. Experimental setup

The present experiments are the first in a series aiming to conclusively explain the resonant collapse. We will extend the work of Lagrange et al. [5] and Meunier et al. [9] using a significantly improved setup. With the recent commissioning of a large rotating platform we can now mount the complete PIV system (laser, camera, computer) along with the precessing cylinder in the rotating frame. This allows us to tilt the laser light sheet with the cylinder and therefore avoid errors at large tilt angles.

In particular, we focus on the question of how much geostrophic (i.e., axisymmetric or mean azimuthal) motion is created by non-linear interaction of the Kelvin modes. Characterizing the geostrophic flow is important because it changes the basic flow, which in turn detunes the resonances of the Kelvin modes. So far, no theory has succeeded in predicting its amplitude or spatial structure. Also, our data will allow validation of accompanying direct numerical simulations [1]. Data were obtained for both the initial transient after commencement of forcing and the steady state long after the tilt.

Experimental Setup and Procedure

Figure 2 shows our experimental setup. A cylinder, filled with water and spinning at Ω_1, is mounted on a DC motor's axis. A rotary encoder measures the motor's angular velocity with an accuracy of 0.1%. The cylinder is made from Perspex and has an inner radius $R = 46.2\,\text{mm} \pm 0.1\,\text{mm}$. Its effective height

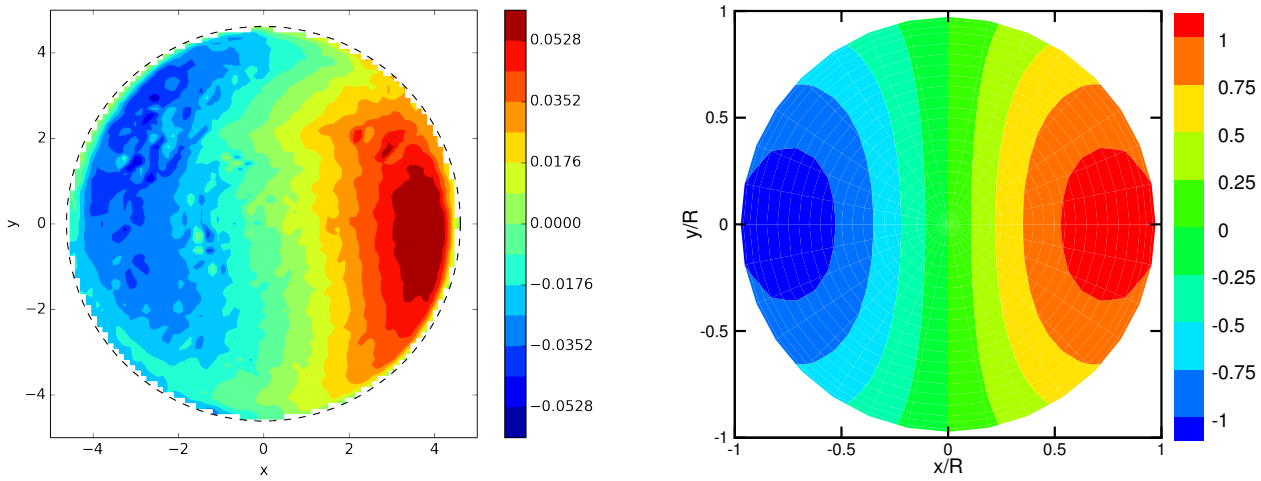

Figure 3. (Left) steady state flow, time averaged axial vorticity, in 1/s; $h = 0.457$, Re $= 2500$, $\omega = 1.886$, $\theta = 2°$. (Right) Theoretical inviscid shape, normalized vorticity.

H can be varied by using different insets. Aligned with the axis and facing the cylinder's top, a Redlake ES 11000 11 megapixel camera records PIV images. Motor, cylinder and camera are mounted on a frame which can be tilted to an angle θ of up to 15° by a linear stepper motor. The accuracy of the tilt angle is 0.1°. A light sheet created by a 250mJ dual-pulse NdYAG laser (Big Sky Laser) and cylindrical lenses is arranged such that it illuminates a cross-section of the tilted cylinder at a height $z_{PIV} = z/H$. The coordinate system is fixed at the centre of the cylinder. Together with a PC controlling the camera, all of the above is mounted on a large platform rotating at Ω_2.

Initially, the cylinder was spinning upright to establish a solid body rotation. After 5 minutes, 10 image pairs of 3100×2672 px were recorded. This would later allow to verify the flow was indeed in solid body rotation initially, and to find the centre of rotation, which is required for the PIV evaluation (outlined below). Then the cylinder was tilted (defining $t = 0$) and 200 image pairs (the maximum permitted by available memory) of the transient flow were recorded at 1 Hz. Once the images were downloaded to the hard disk—about 5 minutes after the tilt—the flow was assumed to have reached a steady state and another 50 image pairs were recorded.

Four dimensionless parameters govern the problem: the forcing amplitude $\varepsilon = \Omega_2 \sin\theta/\Omega$ and frequency $\omega = \Omega_1/\Omega$, the Reynolds number $\mathrm{Re} = \Omega R^2/\nu$, and the cylinder aspect ratio $h = H/R$. Here, $\Omega = \Omega_1 + \Omega_2 \cos\theta$ is the cylinder rotation rate in the laboratory frame of reference.

All experiments reported here were set up to force the (n, l, m) = (1, 1, 1) mode. The first integer n corresponds to an axial wave number $k = (2n-1)h/\pi$ which is chosen such that the Kelvin mode fits exactly into the height of the cylinder and becomes resonant. The second index l denotes the radial wave number, or the branch of the dispersion relation. Finally, precession can only force an azimuthal wave number $m = 1$.

PIV and Data Processing

Although the camera tilts with the cylinder, it is fixed in the table frame of reference and therefore records mainly a solid body rotation. To reveal the secondary flow, the solid body rotation is subtracted by rotating the image pairs before applying the PIV cross-correlation. This removes the large velocity gradients which would otherwise render PIV almost impossible. The time separation between the image pairs was chosen such that the cylinder rotates $\approx 10°$. We found this to be marginal or even too long for large forcing amplitudes; future studies will consider a rotation of $\approx 5°$ instead.

Here, rotating around the correct centre is crucial to not introduce a spurious mean velocity. We apply a semi-automatic procedure to find the centre of rotation using the images recorded before the tilt: the centre is first estimated by fitting an ellipse to the cylinder wall, and then iteratively corrected such that the space and time averaged velocity becomes zero.

The rotated images were then processed by a two-pass cross-correlation algorithm with image shifting/deformation described in [10]. Using 50% overlap and interrogation window sizes of 128 and 64 px, respectively, yields 82×95 velocity vectors. The large window size was chosen to alleviate bad vectors due to the rather long time separation, and hence, large particle displacements between the double images.

Results

We measured at tilt angles of $\theta = 0.5, 2$ and 5° and aspect ratios $h = 0.457, 1, 1.835$ and 2.615. Data at 15° is currently being acquired. The cylinder and platform rotation rates were $0.443 \le \Omega_1 \le 1.886$ rad/s and $0.209 \le \Omega_2 \le \pi/2$ rad/s (maximum rotation rate is 4π rad/s), respectively, yielding Reynolds numbers of $500 \le \mathrm{Re} \le 46\,000$.

For the case $h = 0.457$, Re $= 2500$, $\omega = 1.886$ and $\theta = 2°$, Figure 3 shows contours of axial vorticity of the time-averaged steady state flow in a plane $z_{PIV} = -0.26$. Its structure is no different from the instantanous flow field; no instability is observed nor expected at this Reynolds number. We find a typical (1, 1, 1) mode shape consisting of two counter-rotating vortices. It generally agrees well with linear, inviscid theory shown on the right. The theory predicts a vorticity (and velocity) field symmetric about the y-axis. However, in reality the shape is slightly twisted, which has been already observed in previous studies [2, 9].

For the same case, velocity vectors and contours of velocity magnitude are shown in figure 4. Again, the spatial structure matches the theory very well (not shown). However, in the experiments, we find the position of maximum transverse velocity is slightly shifted to the right, which is even clearer in the normalized velocity profile plotted in figure 5. This indicates a mean azimuthal velocity, i.e., geostrophic flow. It has been ob-

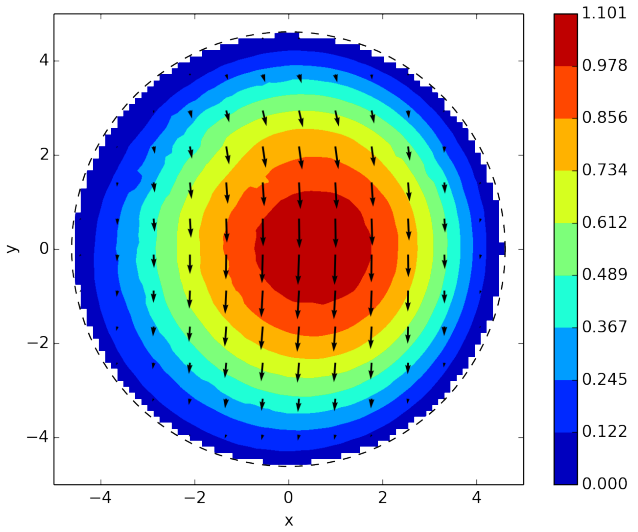

Figure 4. Steady state flow, time averaged sectional velocity field in cm/s, showing every 6$^{\text{th}}$ vector, and contours of velocity magnitude. Same parameters as in figure 3.

served before and is thought to be a nonlinear effect, hence the present observation is consistent with previous work. A slight deviation of the measured velocity near $x/R = \pm 1$ is caused by reflections at the cylinder wall (no image masking was used).

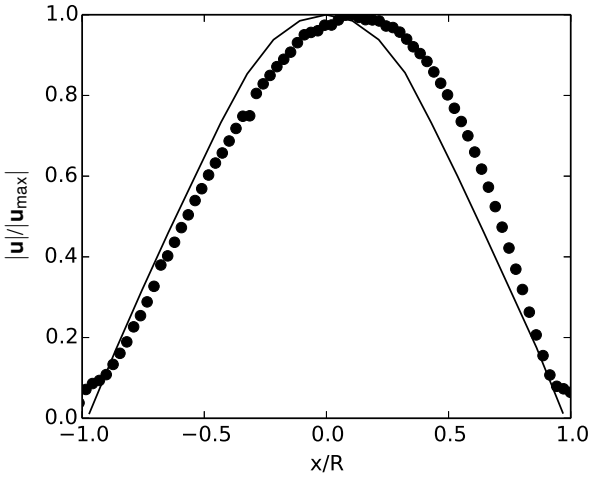

Figure 5. Steady state flow, normalized sectional velocity magnitude along a line at $y = 0$, PIV (symbols) vs. theory (line). Same parameters as in figure 3.

Instantaneous velocity fields were projected onto the theoretical shapes f_i and g_i of the Kelvin modes as described in [9], yielding amplitudes A_i and angles θ_i for the ith mode:

$$(v_r, v_\theta) = \varepsilon\Omega R \sum_{i=1}^{\infty} A_i \cos(k_i z_{PIV}) \begin{bmatrix} f_i(r) \\ g_i(r) \end{bmatrix} e^{j(\theta-\theta_i)} + \text{c. c.} \quad (1)$$

The temporal evolution of the mode amplitude after the tilt is depicted in figure 6. The forced Kelvin mode clearly grows exponentially and reaches a saturation amplitude of -0.4 after about 40 s, while the other mode's amplitudes stay close to zero.

This in agreement with linear, viscous theory, which predicts that at a resonance the forcing term will be balanced by the viscous damping from the boundary layers. The saturation value

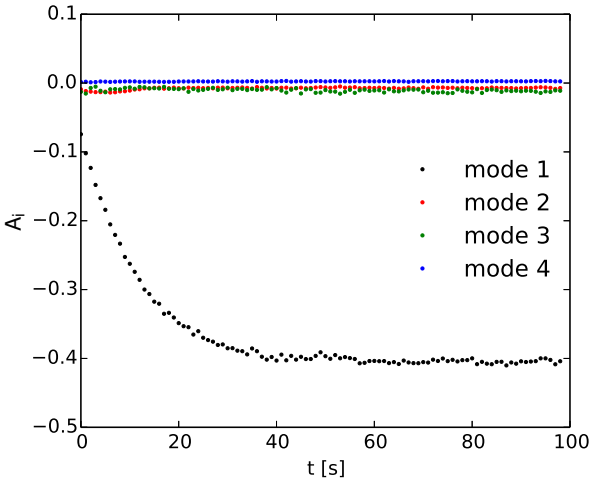

Figure 6. Temporal evolution of the first four Kelvin mode amplitudes after the tilt. Same parameters as in figure 3.

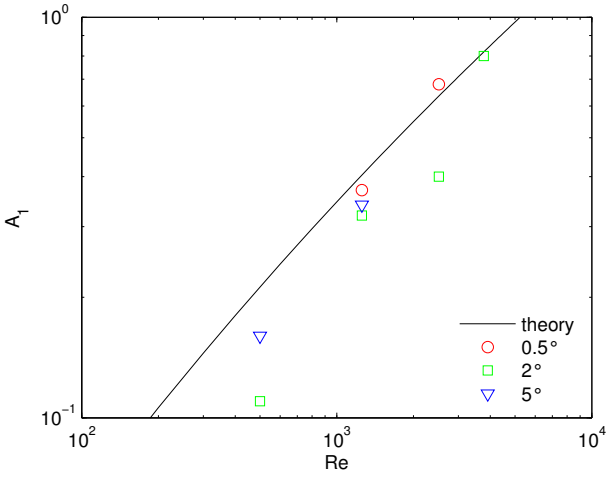

Figure 7. Saturation amplitude of the forced Kelvin mode for $h = 0.457$ at different Re and tilt angles. PIV (symbols) vs. theory (line).

of the amplitude A_1 is extracted for each Reynolds number and tilt angle. This is plotted in figure 7 and compared to the linear, viscous theory of Meunier et al. [9]. The amplitude indeed grows as $\sqrt{\text{Re}}$ because the viscous damping scales as $1/\sqrt{\text{Re}}$. There is a correct quantitative agreement although there is no fitting parameter.

In contrast to Kelvin mode amplitudes, the amplitude A_0 of the geostrophic flow is difficult to quantify. No theory exists for the radial profile, therefore the choice of basis functions to project on would be somewhat arbitrary. Here, we simply define A_0 as the non-dimensionalized maximum value of the azimuthally averaged azimuthal velocity:

$$A_0 = \max_r \left[\frac{1}{\varepsilon\Omega R} \frac{1}{N} \sum_{i=1}^{N} v_{\theta,i}(r) \right] \quad (2)$$

The temporal evolution of A_0 is plotted in figure 8. After the tilt, A_0 grows exponentially just as A_1, also saturating after about 40 s. It appears to follow the trend of mode 1. Note that the corresponding numerical study [1] also shows a correlation between the azimuthal mean flow and mode 1. The radial profile of the geostrophic flow becomes parabolic during the first 10 s with a maximum azimuthal velocity occurring close to

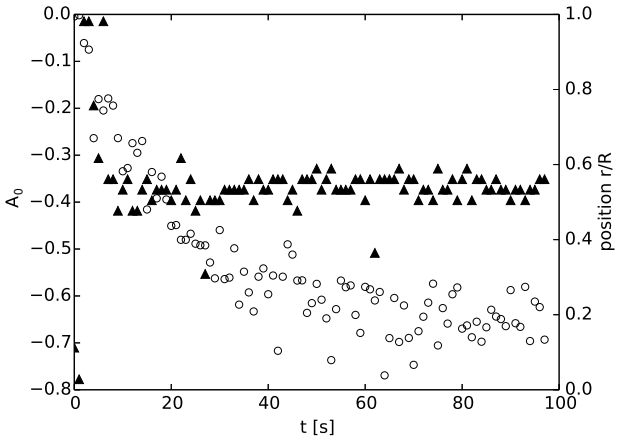

Figure 8. Temporal evolution of the geostrophic flow after the tilt. Circles show the amplitude, i.e., the maximum azimuthal velocity. Its non-dimensional radial position is depicted by the triangles. Same parameters as in figure 3.

$r/R = 0.5$. Thereafter, the flow retains this shape and merely grows in amplitude.

Note that even though A_0 is non-dimensionalized by $\varepsilon\Omega R$, one cannot compare this value directly to the amplitude of the Kelvin modes since their basis functions f_i and g_i may be much larger than unity. In dimensional units, the maximum geostrophic flow for this case is $\approx 0.1\,\mathrm{cm/s}$, which is about 10 times smaller than the maximum transverse velocity caused by the forced Kelvin mode. This also explains the increased noise in the data of figure 8 as compared to figure 6.

Conclusions

We presented new results of an experimental study of precession driven flow in cylinder. Mounting the complete PIV system in the rotating frame allows for accurate measurement even at large tilt angles. Amplitudes of the forced Kelvin modes and of the geostrophic flow are extracted. The amplitude of forced Kelvin modes is in good agreement with the viscous theory in the absence of instability for small tilt angle or Reynolds number. There is a mean azimuthal geostrophic flow which is always retrograde and cannot be predicted by inviscid theory. Future results will allow to give the dependence of this mean azimuthal flow with tilt angle and Reynolds number in both laminar and turbulent regimes. This mean azimuthal flow is very important in rotating flows because it is very often observed although inviscid theories do not predict its existence. It has a large effect on rotating flows as it changes the basic flow and thereby detunes all the possible resonances. Our simple experiment is thus an easy way to characterize this puzzling mechanism of creation of geostrophic motion.

Acknowledgements

We would like to acknowledge financial support from the Australian Research Council through Discovery Program Grant DP130101744. PM would like to thank the French Labex MEC and acknowledges financial support though the ANR Grant 11 BS56 012 01.

References

[1] Blackburn, H. M., Albrecht, T., Manasseh, R., Lopez, J. M. and Meunier, P., Instability in a precessing cylinder flow, in *19th Australasian Fluid Mechanics Conference, Melbourne, Australia*, 2014.

[2] Fabre, D., Sipp, D. and Jacquin, L., Kelvin waves and the singular modes of the Lamb-Oseen vortex, *J. Fluid Mech.*, **551**, 2006, 235–274.

[3] Johnson, L., The precessing cylinder, Notes on the 1967 Summer Study Program in Geophysical Fluid Dynamics at the Woods Hole Oceanographic Inst. Ref. 67–54, 1967.

[4] Kelvin, L., Vibrations of a columnar vortex, *Phil. Mag.*, **10**, 1880, 155–168.

[5] Lagrange, R., Eloy, C., Nadal, F. and Meunier, P., Instability of fluid inside a precessing cylinder, *Phys. Fluids*, **20**, 2008, 081701–1–4.

[6] Malkus, W. V. R., Precession of the earth as the cause of geomagnetism, *Science*, **160**, 1968, 259–264.

[7] Manasseh, R., Breakdown regimes of inertia waves in a precessing cylinder, *J. Fluid Mech.*, **243**, 1992, 261–296.

[8] McEwan, A. D., Inertial oscillations in a rotating fluid cylinder, *J. Fluid Mech.*, **40**, 1970, 603–640.

[9] Meunier, P., Eloy, C., Lagrange, R. and Nadal, F., A rotating fluid cylinder subject to weak precession, *J. Fluid Mech.*, **599**, 2008, 405–440.

[10] Meunier, P. and Leweke, T., Analysis and treatment of errors due to high velocity gradients in particle image velocimetry, *Expts Fluids*, **35**, 2003, 408–421.